Flywheel Energy Storage Supported Adaptive Energy Management Strategy for Solar-powered Electric Vehicle Charging Station

S. Jithin[1,2,*] and T. Rajeev[1]

[1]*College of Engineering Trivandrum, Thiruvananthapuram, Kerala, India*
[2]*A P J Abdul kalam Technological University, Thiruvananthapuram, Kerala, India*
E-mail: d-tve19jan018@cet.ac.in
[*]*Corresponding Author*

Received 26 January 2022; Accepted 18 May 2022;
Publication 03 January 2023

Abstract

The large-scale integration of solar photovoltaic systems and electric vehicles into power systems result in technical challenges due to the volatile nature of the generation and electric vehicle load. The paper presents an energy-storage supported adaptive DC-link voltage regulation based energy management strategy for improving hybrid AC/DC microgrid stability. The proposed volatility based control approach improves hybrid microgrid stability under volatile electric vehicle loading and renewable energy fluctuations. The adaptive energy management strategy limits the overstress on flywheel energy storage depending on the flywheel SoC profile. Different load profiles and source intermittency are considered to analyze the effectiveness of the proposed strategy. The combined control strategy of the interlinking converter and flywheel energy storage in power exchange mode operation and independent mode operation achieve energy balance with the change in solar irradiation and the addition/disconnection of electric vehicles. In addition, real-time experiments are performed to validate the proposed energy

Distributed Generation & Alternative Energy Journal, Vol. 38_2, 669–690.
doi: 10.13052/dgaej2156-3306.38213

management strategy under various volatile conditions. The hybrid AC/DC microgrid with proposed energy management strategy provided a frequency improvement of 0.44% and voltage improvement of 7.5%.

Keywords: Hybrid AC/DC microgrid, electric vehicle charging station, energy management strategy, flywheel storage, solar photovoltaic.

1 Introduction

Electric vehicles (EVs) have gained a lot of attention as viable modes of transportation due to the need for a green and sustainable method of transportation. However, EV adaptability depends on the charging infrastructure [1]. The main disadvantage of EVs is their lower mileage compared to their counterparts. Fast charging stations (FCS) are a way to extend the EV driving range. The FCS can charge an EV in less than thirty minutes. FCS is mainly DC and operates on a higher DC voltage. The benefits of higher charging voltage are reduced charging time, increased power retention capacity, and lower weight [2]. The charging voltage of 800 V is expected to be a de-facto standard globally by 2026. The charging standards are CHAdeMO, GB/T, combined charging system (CCS), IEC 61851, and SAE J1772 [3]. However, an electric vehicle charging station (EVCS) characteristics as a load are highly volatile. The factors such as charging duration, the unpredictability of power requirement of EV, and large fluctuations of current due to EVCS charging cause violations of grid constraints [4]. Hence, the large-scale integration of EVCS and its effects on the distribution network has become a hot topic.

The advent of renewable energy sources (RES) and the advancement of energy storage technologies helps to mitigate the congestion in the existing grid due to large-scale EV penetration [5]. However, the integration of solar and EVs into power systems is fraught with technical challenges due to generation intermittency and increased load. Large-scale photovoltaic (PV) installations can cause over-generation during light load, while large EV installations can cause overload during peak load. As a result, voltages and frequencies fluctuate, losses increase, and power quality degrades. When such issues are not addressed, the power system stability is negatively affected, resulting in time-consuming and costly grid reinforcement [6, 7]. The practical solution is a hybrid AC/DC microgrid (HMG) implemented by deploying small AC and DC grids within the existing grid. Interlinking converter (IC) connects the AC and DC grids in an HMG. The HMG will play a significant

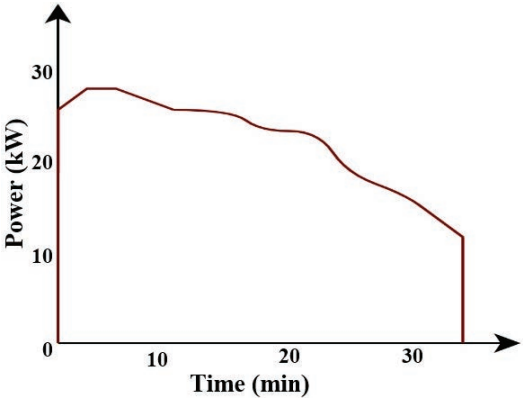

Figure 1 Power curve of 30 kW charger.

role in future energy systems. The AC/DC energy conversions are reduced in a hybrid microgrid, which improves efficiency [8].

India has a vast potential for solar energy. Globally, India is in 5^{th} position in terms of installed solar capacity. Hence solar-powered EVCS have an extensive spectrum in the Indian scenario. In India, for DC FCS, the standards specified are Bharat EV DC001 and DC002. The maximum voltage rating of DC002 is 1000 V, and the power output is 30 kW to 150 kW [9]. Random EV charging activity generates a high-power impulse. The typical power curve of a real 30 kW charger in a charging period is shown in Figure 1 [10]. The impact of FCS is compensated by a solar-powered EVCS integrated with an energy storage system (ESS). The addition of ESS to the FCS will raise the share of solar energy delivered to EVs while improving the microgrid's resilience to the intrinsic intermittency of PV output and a high degree of deregulation on the demand side [11]. The flywheel energy storage system (FESS) is one of the most suitable types of ESS due to its high power density and moderate energy density. It can thus accommodate sudden load fluctuations and long-term storage requirements [12].

The integration of EVCS with RES and the grid creates challenges for energy management in the overall microgrid. A PSO-based energy management strategy (EMS) for grid-tied PV-battery system of EV charging is discussed in [13], which requires pre-known forecast data for optimization. EMS of solar EVCS for workplaces using Gaussian charging profile is analyzed [14]. A fuzzy-based PMS [15] and a rule-based EMS [16] developed for PV-EVCS are microgrid-specific and not generalized. A centralized EMS for the PV-EVCS proposed in [17] relies on low bandwidth communication

and affects gain tuning. A DC-link voltage regulation-based EMS presented in [18] uses the DC-link voltage information for coordination PV-EVCS. The shortcoming of the strategy is it does not consider the ESS. A decentralized EMS suitable for volatile loading conditions and during power fluctuations of RESs in the grid is an area where various researchers are working. An adaptive EMS is required for the IC to improve the HMG stability under volatile EV loading and RES power fluctuations. The research gaps identified are:

1. The conventional distribution network can support EV integration up to only 25% of the rated capacity. On the other hand, the DC microgrid operates stably up to 70% of EVCS integration [19]. However, a complete switch-over from the existing AC distribution network to the DC microgrid is not practically viable. The suitability of HMG for large-scale EVCS integration is rarely analyzed.
2. The existing EMS primarily concentrates on power-sharing due to traditional load switching in HMG. Since the characteristics of EVCS switching are highly volatile and due to the scattered nature of EVCS, a proper decentralized control strategy is essential.
3. The future control scheme should accomplish the expected functionality with an easy control scheme rather than complex control schemes. Also, safer, quicker, reliable, and economical testing methods such as real-time simulations and hardware-in-the-loop technologies to test the practical feasibility of the control schemes are required.

This paper presents a novel EMS to enhance HMG stability. The significant contributions of this article are as follows:

1. A competent and practical HMG architecture for large-scale EVCS integration where the DC microgrid is dedicated exclusively for EVCS integration.
2. A DC-link voltage regulation-based EMS for accurate power-sharing between PV, EVCS, FESS, and AC microgrid as a promising solution for large-scale EVCS integration.
3. The adaptive flywheel state of charge (SoC) EMS limits the overstress on FESS.
4. Real-time verification of the proposed EMS using OPAL-RT.

The rest of the paper is organized as follows: In Section 2, HMG system configuration and modeling are presented. The general formulation of EMS for solar-powered EVCS with FESS is described in Section 3. In Section 4, simulation analysis and real-time verification are presented to demonstrate the effectiveness of EMS. Finally, Section 5 presents the concluding remarks.

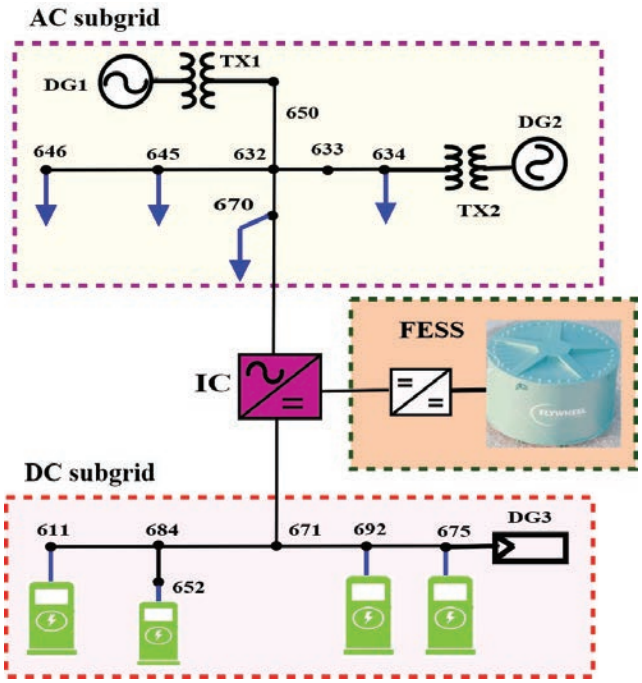

Figure 2 Hybrid AC/DC microgrid.

2 System Configuration

Figure 2 shows the simplified single-line diagram of the HMG considered in this paper. It consists of an AC subgrid and a DC subgrid interconnected through an IC. The DGs and loads are distributed in the AC subgrid, and the DC subgrid is exclusively for solar powered EVCS. The integration of EVCS and PV in the DC subgrid minimizes the conversion losses and improves the HMG efficiency. The IC operates as either an inverter or a rectifier depending on the operating mode. The FESS is connected to the DC-link of IC. The IC and FESS, as a single unit, ensure the energy management within the HMG. IC is provided with three nested control loops (i.e., power, voltage, and current loop). The IC is operated using a virtual synchronous machine-transient (VSM-T) controller. The ability of VSM to emulate inertia improves frequency stability. The transient controller is a lead compensator used to enhance the transient characteristics. The lead network does not disturb the steady-state error. Hence, the steady-state performance provided by VSM is preserved. The details of the VSM-T controller employed in the microgrid

is reported through our previous work [20]. Compared to other high power density ESS, FESS also has a better energy density. Hence, the FESS supports sudden load fluctuations as well it provides long-term support. The total capacity of the FESS is given by,

$$E_F = \frac{1}{2} I(\omega_{max}^2 - \omega_{min}^2) \tag{1}$$

where I is the moment of inertia of the flywheel, ω_{max} is the rated speed of flywheel and ω_{min} is the minimum speed of the flywheel. The effective stored energy of flywheel is used within these two speeds. The energy stored in the FESS is modified as in Equation (2).

$$\begin{aligned} E_F &= \frac{1}{2} I \omega_{max}^2 (1 - k_\omega^2) \\ where,\ k_\omega &= \frac{\omega_{min}}{\omega_{max}} \end{aligned} \tag{2}$$

The ratio k_ω determines the percentage of stored energy extracted from the flywheel. A reasonable choice is $k_\omega = 0.5$, which provides 75% energy utilization [12]. High-speed flywheels are employed to increase the energy storage capacity. This approach allows a reduction in the size of FESS as the moment of inertia can be kept smaller. The flywheel state of charge [21] is computed as,

$$SoC_F = \frac{\omega_F(t)}{\omega_{max}} \times 100\% \tag{3}$$

where $\omega_F(t)$ is the is the energy stored in the flywheel at the current instant. The operating range of flywheel is chosen as 20% to 90% of flywheel SoC to avoid the complete discharge and overcharging.

3 Energy Management Strategy

The EMS of the HMG is based on DC-link voltage regulation. During the steady-state operation of HMG, it satisfies the following criteria:

$$P_{PV} \pm P_F \pm P_{AC} - P_{EV} - P_L = 0 \tag{4}$$

where P_{PV}, P_F, P_{AC}, P_{EV}, and P_L are the PV power, flywheel power, AC subgrid power, EV power, and AC load power, respectively. It is considered that the EVCS operates in grid-to-vehicle mode only. In Equation (4), the positive sign represents the power supplied and negative sign is for power

consumption. During the irradiance change, a sequence of events ensue to acquire energy equilibrium in the system.

$$\begin{aligned} Solar\ irradiance\uparrow\downarrow \rightarrow P_{PV}\uparrow\downarrow \rightarrow Power\ at\ DC-link\uparrow\downarrow \\ \rightarrow V_{dc}\uparrow\downarrow \rightarrow V_{dc}\ regulation \rightarrow i_{dc,h}\downarrow\uparrow \end{aligned} \tag{5}$$

where V_{dc} is the DC-link voltage and $i_{dc,h}$ is the reference current generated in the hybrid mode of operation. With the addition/disconnection of EVs, the series of events happen to achieve the energy balance in the system are,

$$\begin{aligned} Charging\ Power\uparrow\downarrow \rightarrow I_{EV}\uparrow\downarrow \rightarrow Power\ at\ DC-link\downarrow\uparrow \\ \rightarrow V_{dc}\downarrow\uparrow \rightarrow V_{dc}\ regulation \rightarrow i_{dc,h}\uparrow\downarrow \end{aligned} \tag{6}$$

where I_{EV} is the current drawn by the EV. The value of $i_{dc,h}$ is computed based on the flywheel SoC and excess power availability from the AC subgrid. If the flywheel SoC is greater than 70%, then $i_{dc,h}$ depends on FESS. If the flywheel SoC is in between 20% to 70%, then $i_{dc,h}$ is computed based on AC subgrid and FESS conditions. $i_{dc,h}$ solely depends on AC subgrid power when flywheel SoC is below 20%. The $i_{dc,h}$ for different cases is computed using Equation (7).

$$i_{dc,h} = \begin{cases} \frac{P_F^*}{v_{dc}^*} & SoC_F > 70\% \\ \frac{P_{IC}^* - P_F^*}{v_{dc}^*} & 20\% < SoC_F < 70\% \\ \frac{P_{IC}^*}{v_{dc}^*} & SoC_F < 20\ \% \end{cases} \tag{7}$$

During the independent operation mode of subgrids, the energy balance at the DC subgrid and AC subgrid is given by,

$$\begin{aligned} P_{PV} \pm P_F - P_{EV} = 0\ DC\ subgrid \\ P_{AC} - P_L = 0\ AC\ subgrid \end{aligned} \tag{8}$$

Similar to the power exchange mode operation, the series of events occurring in independent mode operation to achieve energy balance with the change in solar irradiation and with the addition/disconnection of EVs are:

$$\begin{aligned} Solar\ irradiance\uparrow\downarrow \rightarrow P_{PV}\uparrow\downarrow \rightarrow Power\ at\ DC-link\uparrow\downarrow \\ \rightarrow V_{dc}\uparrow\downarrow \rightarrow V_{dc}\ regulation \rightarrow i_{dc,s}\downarrow\uparrow \end{aligned} \tag{9}$$

$$\begin{aligned} Charging\ Power\uparrow\downarrow \rightarrow I_{EV}\uparrow\downarrow \rightarrow Power\ at\ DC-link\downarrow\uparrow \\ \rightarrow V_{dc}\downarrow\uparrow \rightarrow V_{dc}\ regulation \rightarrow i_{dc,s}\uparrow\downarrow \end{aligned} \tag{10}$$

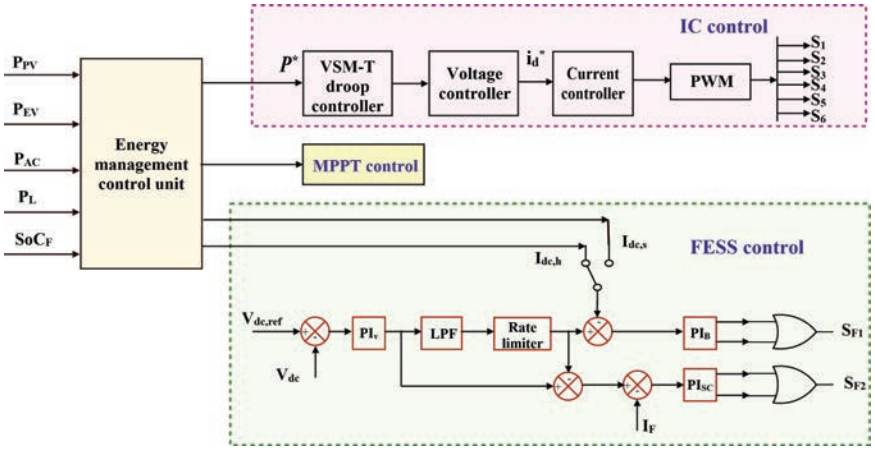

Figure 3 Combined control strategy.

where $i_{dc,s}$ is the reference current generated in independent mode of operation and is computed as follows:

$$i_{dc,s} = \begin{cases} \frac{P_{PV}-P_{EV}}{v_{dc}^*} & 20\% < SoC_F \\ 0 & SoC_F < 20\ \% \end{cases} \tag{11}$$

The combined control strategy of the IC and FESS is shown in Figure 3. In independent operation mode, the FESS compensates for the DC-link voltage fluctuations, by supplying/absorbing the shortfall/excess of power in the DC subgrid. However, in the power exchange mode through IC, the AC subgrid and FESS compensate for the DC-link voltage fluctuations. The power to be imported/exported from the AC subgrid is decided based on the SoC of FESS. The desired power transfer through IC (P_{IC}) is a function of flywheel SoC and can be written as,

$$P_{IC} = \begin{cases} 0 & SoC_F > 70\% \\ (P_L - P_{PV})(SoC_F) & 20\% < SoC_F < 70\% \\ (P_L - P_{PV}) & SoC_F < 20\ \% \end{cases} \tag{12}$$

The power transfer as in Equation (12) decides the power to be fed from the FESS and the AC subgrid based on the flywheel SoC and EVCS power demand. Therefore, when the FESS SoC is less, more power is imported from the AC subgrid through IC and vice-versa. The energy management control unit algorithm is given in Table 1.

Table 1 Energy management control unit algorithm

Algorithm for energy management control unit
Step 1: Read the input data : P_{PV},P_{AC},P_L,P_{EV},SoC_F
Step 2: Decide the operating mode of HMG
if P_{AC}-P_L=0 : *Independent operation of IC* $\Rightarrow$ **Go to step 3**
else : *Power exchange through IC* $\Rightarrow$ **Go to step 4**
Step 3: Sub problem for independent operation
Compute ΔP=P_{PV}-P_{EV}
While $\Delta P > 0$
if $SoC_F < 0.9$: *Charge FESS*
else : *MPPT control (Derate MPPT)*
end
end
While $\Delta P < 0$
if $SoC_F > 0.2$: *Discharge FESS*
else : *Disable charger*
end
end
Step 4: Sub problem for power exchange through IC
Compute ΔP=P_{PV}-P_{EV}
While $\Delta P > 0$
if $SoC_F < 0.9$: *Charge FESS*
else if (P_{AC}-P_L)< 0 : *Inverter mode operation of IC*
else : *MPPT control (Derate MPPT)*
end
end
While $\Delta P < 0$
if $SoC_F > 0.7$: *Discharge FESS*
else if $0.2<SoC_F<0.7$ & (P_{AC}-P_L)> 0 : *Shortage of power from AC subgrid & FESS*
else if $0.2<SoC_F<0.7$ & (P_{AC}-P_L)< 0 : *Discharge FESS*
else if $SoC_F <0.2$ & (P_{AC}-P_L)> 0 : *Rectifier mode operation of IC*
else : *Disable charger*
end
end
Step 5: Stop

4 Simulation Experiment and Results

To verify the effectiveness of the proposed EMS, time domain simulation in MATLAB/Simulink and real-time case studies using OPAL-RT are performed. In addition, the performance of EVCS integration is analyzed under variable irradiation and PV outage on a modified IEEE 13-bus HMG test system. Simulation is carried out for 10 seconds. As the focus is on the

Table 2 Simulation parameters

Parameter	Value
Nominal AC voltage	415 V(l-l)
Nominal frequency	50 Hz
Nominal DC voltage	800 V
Switching frequency	5 kHz
Cut-off frequency	5 Hz
PV capacity	40 kW
Diesel generator capacity	30 kVA
FESS capacity	30 kWh
Flywheel speed	32000 rpm
EVCS rating	30 kW
Filter capacitor	65 μF
Filter inductor	1.8 mH
VSM damping coefficient	4
VSM mechanical time constant	2 s
VSM-transient controller time constants	0.02. 0.005

solar-powered EVCS placed on the DC subgrid, the inverter operation of the IC is not considered in simulation analysis. It should be noted that the IC can operate in inverter mode, if DC subgrid has excess generation.

4.1 Time Domain Simulation

The capacity of the HMG considered is 100 kW. It consists of two DGs in the AC subgrid and a PV in the DC subgrid as sources. The simulation parameters are given in Table 2. The duration and test conditions are given in Table 3. The DC subgrid is developed exclusively for the EVCS, and loads are connected to the AC subgrid. Initially, no EVCS is connected to the DC subgrid, and hence the load at the DC subgrid is zero. The AC subgrid load is (33+j15) kVA. Assuming a diversity factor of 1.8 for the AC subgrid, it has a reserve capacity of about 27 kW. Therefore, the maximum power that can be transferred through the IC is limited to 30 kW.

For the duration t = 0 to 5.2 s, both the subgrids operate independently, and power exchange mode for the duration t = 5.2 to 10 s, as illustrated in Figure 4. For t = 0 to 2 s, the EVCS load at the DC subgrid is zero. The PV output power is utilized to charge the FESS. For t = 2 to 4 s, an EVCS is switched. The flywheel continues charging as PV power is greater than the EVCS power. The change in irradiation changes the PV power, which in turn changes the charging power of FESS accordingly. For t = 4

Table 3 Test conditions

Period (s)	Irradiation W/m^2	EVCS load (kW)
0-1	1000	0
1-2	800	0
2-3	800	30
3-4	1000	30
4-5	1000	60
5-6	800	60
6-7	1000	90
7-8	1000	90
8-9	0	120
9-10	1000	120

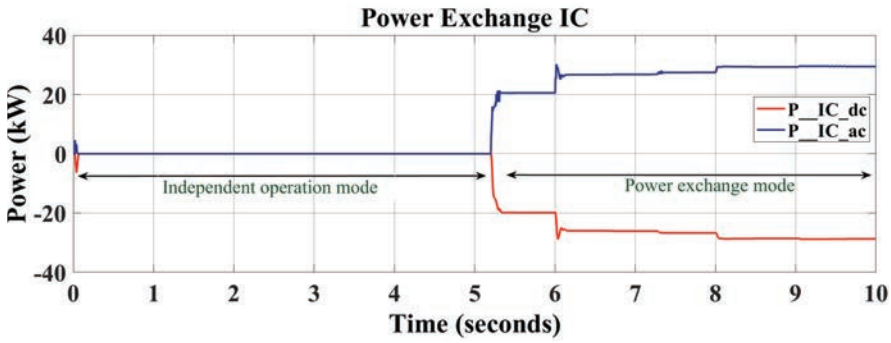

Figure 4 Power exchange through IC.

to 5 s, another EVCS is added. PV power is insufficient to meet the increased demand, so the FESS discharges. At instant 5.2 s, the SoC of the FESS falls below 70%, switching the operation to power exchange mode. In this mode, the FESS and AC subgrid work together to supply power to the EVCS. The FESS charging/discharging power, EVCS power, and PV power are shown in Figure 5. The SoC profile of the flywheel is shown in Figure 6.

The DC subgrid voltage, the AC subgrid RMS voltage, and the AC subgrid frequency is shown in Figure 7. The voltages and frequency are maintained within limits as per the IEEE 1547 standard. As per IEEE 1547 standard, the allowable voltage variation is $\pm 10\%$, and frequency variation is $\pm 2\%$. The power supplied by FESS, power imported from the AC subgrid, and the percentage variation of voltage in the DC and AC subgrids of the HMG based on the test conditions is tabulated in Table 4. Flywheel power is negative when the FESS is charging and vice-versa. The voltage variation

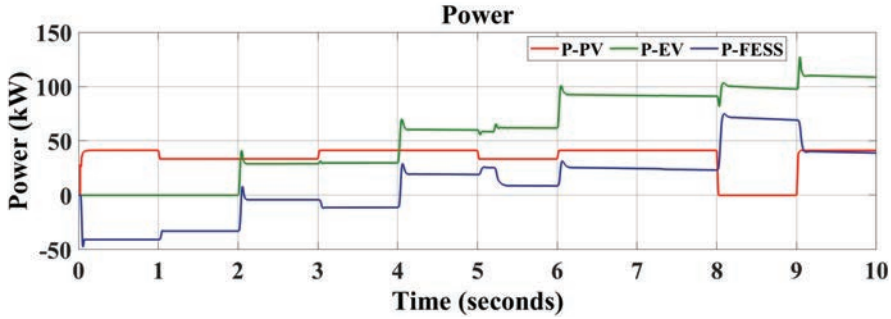

Figure 5 PV power, EVCS power, & flywheel power.

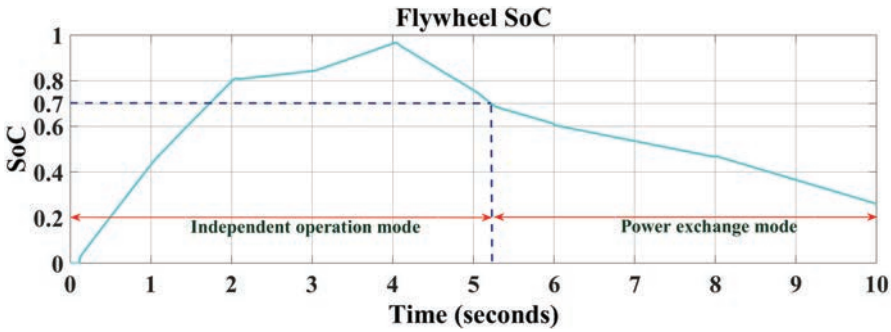

Figure 6 Flywheel SoC.

is negative when the voltage is higher than the nominal voltage. Voltage variations in the subgrids are very minimal. In the instant t = 8 to 9 s, the PV Power is zero representing a solar outage caused by zero irradiation in the nighttime or panel faults. The EVCS loading is also extreme in this duration as all four EVCS are charging. The FESS and AC subgrid together maintain stability in this case. The total power is insufficient, and the EVCSs are charged with reduced power without violating the stability constraints of the HMG. It is important to note that a minor reduction in the charging power will not deteriorate the operation of EVCS, as EV charging power is not a constant, as illustrated in Figure 1.

Different operating scenarios, as described below are considered to illustrate the effectiveness of the proposed SoC-based adaptive EMS. The results are tabulated in Table 7.

- Case 1: PV generation is greater than EVCS capacity and SoC_F is less than 90%.

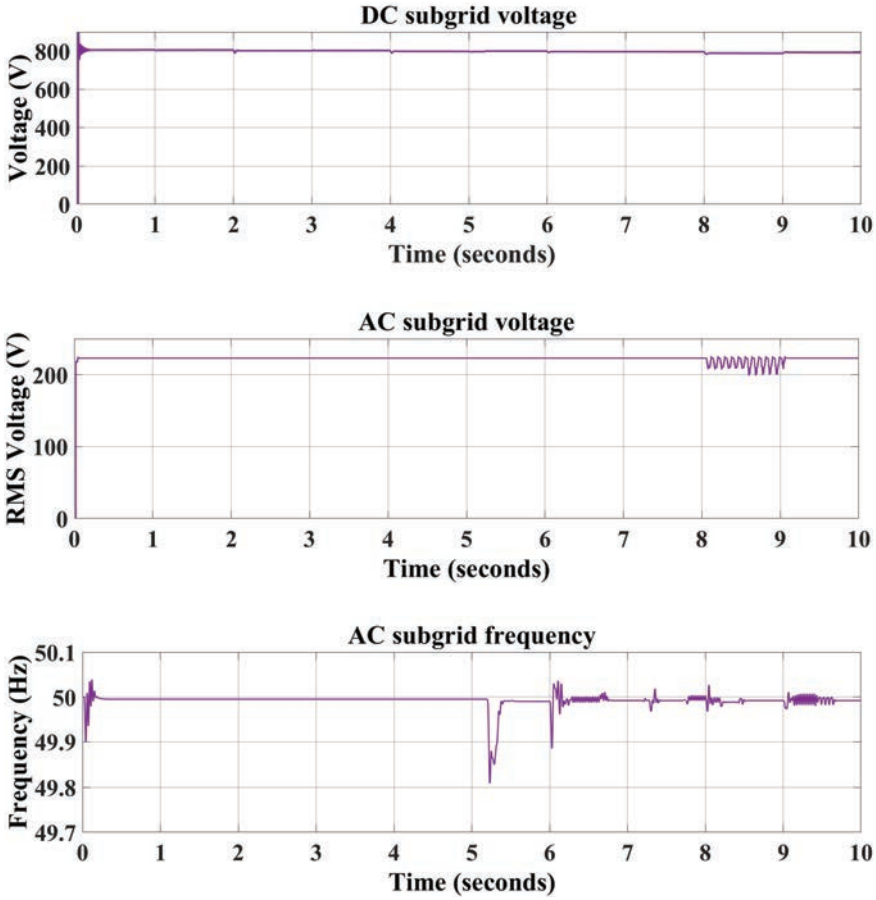

Figure 7 Voltage and frequency of HMG.

- Case 2: PV generation is greater than EVCS capacity and SoC_F is greater than 90%.
- Case 3: PV generation is less than EVCS capacity and SoC_F is greater than 70%
- Case 4a: PV generation is less than EVCS capacity and SoC_F is between 70% and 20%.
- Case 4b: Fluctuating PV generation with SoC_F is between 70% and 20%.
- Case 5: PV generation is less than EVCS capacity and SoC_F is between 20%.

Table 4 Test condition results

Period (s)	Flywheel Power (W/m^2)	Imported AC Subgrid Power (kW)	DC Subgrid Voltage Variation (%)	AC Subgrid Voltage Variation (%)	
0-1	−40	0	−0.63	–	
1-2	−33	0	−0.63	–	
2-3	−4	0	0.5	–	Independent
3-4	−11	0	−0.37	–	operation
4-5	20	0	1.25	–	mode
5-5.2	25	0	0.37	–	
5.2-6	9	20	0	0.26	
6-7	25	26	0.5	0.26	Power
7-8	25	26	0.5	0.52	exchange
8-9	71	29	1.38	6.66	mode
9-10	40	29	0.94	0.52	

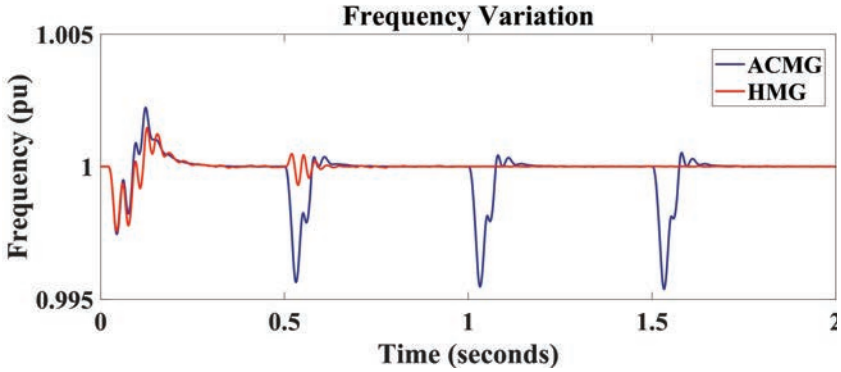

Figure 8 Frequency profile of AC microgrid and HMG with EVCS integration.

The results illustrate that energy management takes place based on the FESS SoC profile. When FESS SoC is above 70%, FESS alone meets the excess EVCS load requirement. As the SoC of FESS decreases, the power delivered by FESS decreases, and the additional power to meet the load is imported from the AC subgrid. As a result, the power share from the AC subgrid is increased, corresponding to the flywheel SoC decrease, thereby reducing overstress of FESS. The power shared by FESS and the AC subgrid during PV generation intermittency also shows the effectiveness of the proposed EMS. Figure 8 shows the frequency profile comparison when EVCS is incorporated into the AC microgrid and HMG. The frequency fluctuations are

Table 5 EVCS switching in AC microgrid

Percentage Loading (%)	Percentage Loading with EV (%)	Voltage Variation (%)	Frequency Variation (%)	Simultaneous Switching	
				Voltage variation (%)	Frequency variation (%)
25	40	2	0.45	14.5	0.49
	55	6.5			
	70	13			
50	65	5	0.45	18.5	0.49
	80	11			
	95	14.2			
75	90	12	0.46	22.3	0.5
	105	17			

Table 6 EVCS switching in HMG

Percentage Loading (%)	Percentage Loading with EV (%)	AC sub-grid		Voltage Variation DC Sub-grid (%)	Simultaneous Switching		
		Voltage Variation (%)	Frequency Variation (%)		AC Voltage Variation (%)	Frequency Variation (%)	DC Voltage Variation (%)
25	40	1	0.03	0.2	2.5	0.2	1.5
	55	2.5	0.14	0.3			
	70	3.5	0.16	0.6			
50	65	5	0.135	0.5	8	0.25	2
	80	5.5	0.14	0.7			
	95	8	0.16	0.7			
75	90	7.2	0.12	1.5	10	0.25	3.4
	105	9.5	0.25	2			

more in the case of the AC microgrid. The HMG provided a better frequency profile. Similarly, the voltage fluctuations are also minimized when EVCS is integrated with the HMG. The frequency and voltage variations for the same loading conditions for the AC microgrid and HMG are tabulated in Tables 5 and 6. The HMG with proposed EMS provided a frequency improvement of 0.44% and voltage improvement of 7.5% compared to EVCS integration in the AC microgrid.

With large-scale EVCS deployment, the HMG provides stable performance for both AC and DC subgrids. The proposed EMS is tested with extreme test scenarios and found to provide satisfactory results. The results validate that the HMG is an effective solution for large-scale EVCS integration. The effectiveness of the proposed EMS for the solar-powered EVCS with FESS is further investigated from the real-time experiments.

4.2 Case Study Using OPAL RT

The proposed controller is validated by considering the realistic data of a 13 bus microgrid system. Data for the sources incorporated were the real

Table 7 FESS power-sharing under various operating scenarios

Operating Scenarios	PV Power	EVCS Capacity	SoC	FESS Contribution	AC Subgrid Contribution	Remarks
Case 1	40	30	<90	−10	0	Charge FESS
Case 2	40	30	>90	0	0	Derate MPPT
Case 3	40	60	>70	20	0	Discharge FESS
Case 4a	40	60	60	12	8	FESS and AC subgrid power
	40	60	40	8	12	
	40	60	25	5	15	
Case 4b	35	60	60	15	10	FESS and AC subgrid power
	30	60	40	12	18	
	25	60	25	9	26	
	30	90	60	36	24	
Case 5	40	60	<20	0	20	Rectifier Mode Disable charger/Reduced power charging
	40	90	<20	0	30	

(a) OPAL-RT real-time experimental setup

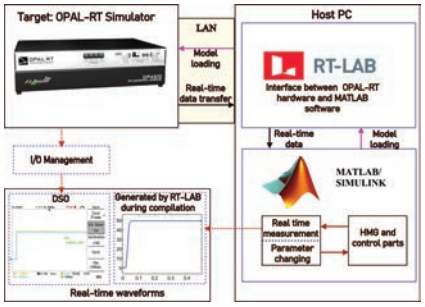

(b) Real-time simulation process using OPAL-RT digital simulator

Figure 9 RTDS using OPAL-RT.

system data of the PV and generator installed at the college of engineering, Trivandrum. The effectiveness of the proposed controller is demonstrated through real-time simulations using OPAL-RT OP4510. OPAL-RT allows testing of control system hardware even when the physical plant or system is unavailable. Furthermore, as the characteristics of solar PV generation are uncertain and to account for the highly non-linear behavior of EVCS, OPAL-RT provides a flexible solution to investigate various testing scenarios in real-time. Figure 9a shows the experimental setup, and it consists of OPAL-RT simulator OP4510 as the target, the host PC, and the LAN networking cable. OP4510 has Intel Xeon E3, 4 core, 3.5 GHz processors. It renders programmable I/O management, managed by fast Xilinx Kintex-7

FPGA. RT-LAB software version 2020.4.1.166 acts as an interface between the OPAL-RT digital simulator and MATLAB. Figure 9b shows the RTDS process. First the MATLAB/Simulink model is loaded to OPAL-RT through RT-LAB to simulate the HMG and proposed controller in real-time. The Simulink model is divided into two subsystems: master and console. The master subsystem consists of the entire HMG and associated controllers. Displays and changeable control parameters are placed in the console and are accessed during RTDS. After model loading and real-time data receiving, real-time waveforms are captured in the host PC and DSO. The same test scenarios of the simulation experiment are considered for RTDS using OPAL-RT.

Case 1: Independent operation of subgrids

Each subgrid of the HMG operates independently when the solar PV has sufficient power to meet the EVCS load demand. In the case of PV power insufficient to meet EVCS load, flywheel energy alone is used to meet EVCS load until flywheel SOC reaches 70%. The PV provides the required power when the first EVCS is switched at time instants t = 2 s. The increased load requirement at t = 4 s with the addition of another EVCS is met by PV and FESS up to t = 5.2 s. Both subgrids are operating independently up to 5.2 s, and the net power exchange through the IC is zero as shown in Figure 10a. The subgrid voltage profiles and AC subgrid frequency are shown in Figure 10b–10d.

Case 2: Power exchange between subgrids

The power exchange mode is activated if the PV does not produce enough power to meet the EVCS load demand and the flywheel SoC is below 70%. The EVCS load is met by PV, flywheel, and AC subgrid power in this mode. At t = 5.2 s, the flywheel SoC reaches 70% and initiates the power exchange mode. The net power exchange through the IC is 20 kW, as shown in Figure 10a. The addition of EVCS at t = 6 s and t = 8 s increases the power drawn from the AC subgrid to 27 kW and 29 kW, respectively. The real-time test results validate the suitability of the proposed EMS for large-scale deployment of EVCS in the HMG.

4.3 Comparative Analysis of Proposed EMS

The analysis with the proposed EMS considers an solar-powered EVCS with FESS. The results are compared with solar-powered EVCS without an

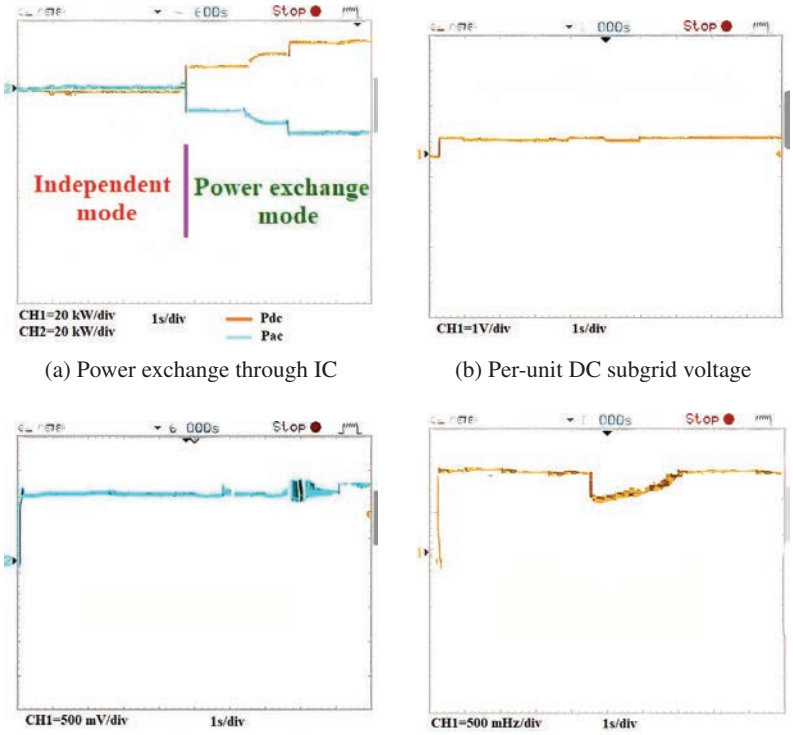

(a) Power exchange through IC

(b) Per-unit DC subgrid voltage

(c) Per-unit AC subgrid RMS voltage

(d) Per-unit AC subgrid frequency

Figure 10 Real-time results: DSO waveforms.

ESS [18]. The comparative analysis results are summarized as follows:

- The strategy in [18] does not consider an ESS. Hence disturbances introduced by EVCS load volatility affect the AC and DC subgrids in solar-powered EVCS without ESS. The proposed strategy with FESS compensates for the load volatility by its quick action, thereby limiting the voltage and frequency fluctuations to minimal.
- The flywheel SoC-based EMS avoids the overloading on the AC subgrid and in the FESS based on system conditions. This approach enhances the HMG performance.

5 Conclusion

This paper presents an energy management strategy for the solar-powered electric vehicle charging station in a commercial hybrid AC/DC microgrid.

The DC subgrid of the hybrid AC/DC microgrid is exclusively provided for an EV charging station. A flywheel energy storage system is integrated with the DC subgrid to tackle the generation intermittency of PV and the highly volatile load characteristics of the EVCS. The HMG with proposed EMS provided a frequency improvement of 0.44% and voltage improvement of 7.5% compared to EVCS integration in the AC microgrid. The proposed EMS can support large-scale EVCS implementation without restructuring the existing power grid. The proposed EMS is based on the SoC profile of FESS and limits the overstress on the flywheel based on system conditions. The SoC-based adaptive EMS improves power-sharing between subgrids and enhances steady-state and transient responses. The simulation analysis and real-time experiments validate the effectiveness of the energy management strategy. Hence, these findings would be pertinent since the hybrid microgrids with solar-powered electric vehicle charging stations are best suited for the large-scale integration of electric vehicles.

References

[1] Tianjin Chen, Xiao-Ping Zhang, Jianji Wang, Jianing Li, Cong Wu, Mingzhu Hu, and Huiping Bian. A review on electric vehicle charging infrastructure development in the uk. *Journal of Modern Power Systems and Clean Energy*, 8(2):193–205, 2020.

[2] Hossam A. Gabbar, Yasser Elsayed, Abu Bakar Siddique, Abdalrahman Elshora, and Ajibola Adeleke. Design of fast charging station with energy management for ebuses. *Vehicles*, 3(4):807–820, 2021.

[3] Jeykishan Kumar K, Sudhir Kumar, and Nandakumar V.S. Standards for electric vehicle charging stations in india: A review. *Energy Storage*, page e261, 2021. 10.1002/est2.261.

[4] Hemakumar Reddy Galiveeti, Arup Kumar Goswami, and Nalin B. Dev Choudhury. Impact of plug-in electric vehicles and distributed generation on reliability of distribution systems. *Engineering Science and Technology, an International Journal*, 21(1):50–59, 2018. 10.1016/j.jestch.2018.01.005.

[5] Rahman M S, Hossain J, Lu J, and Pota H R. A need-based distributed coordination strategy for ev storages in a commercial hybrid ac/dc microgrid with an improved interlinking converter control topology. *IEEE Transactions on Energy Conversion*, 33:1372–1383, 2018.

[6] Alonzo Sierra, Cihan Gercek, Karst Geurs, and Angèle Reinders. Technical, financial, and environmental feasibility analysis of photovoltaic

ev charging stations with energy storage in china and the united states. *IEEE Journal of Photovoltaics*, 10(6):1892–1899, 2020. 10.1109/JPHOTOV.2020.3019955.

[7] Arwa O. Erick and Komla A. Folly. Power flow management in multi-source electric vehicle charging station. *IFAC-PapersOnLine*, 53(2):12590–12595, 2020. 21st IFAC World Congress.

[8] Moudud Ahmed, Lasantha Meegahapola, Arash Vahidnia, and Manoj Datta. Stability and control aspects of microgrid architectures a comprehensive review. *IEEE Access*, 8:144730–144766, 2020. 10.1109/ACCESS.2020.3014977.

[9] Ministry of Power Government of India. Charging infrastructure for electric vehicles (ev) – the revised consolidated guidelines & standards. Technical report, Jan 2022.

[10] Shrey Verma, Shubham Mishra, Ambar Gaur, Subhankar Chowdhury, Subhashree Mohapatra, Gaurav Dwivedi, and Puneet Verma. A comprehensive review on energy storage in hybrid electric vehicle. *Journal of Traffic and Transportation Engineering (English Edition)*, 8(5):621–637, 2021.

[11] Karima Kouka, Abdelkarim Masmoudi, Achraf Abdelkafi, and Lotfi Krichen. Dynamic energy management of an electric vehicle charging station using photovoltaic power. *Sustainable Energy, Grids and Networks*, 24:100402, 2020. 10.1016/j.segan.2020.100402.

[12] Subhashree Choudhury. Flywheel energy storage systems: A critical review on technologies, applications, and future prospects. *International Transactions on Electrical Energy Systems*, 31(9):e13024, 2021.

[13] Qiongjie Dai, Jicheng Liu, and Qiushuang Wei. Optimal photovoltaic/battery energy storage/electric vehicle charging station design based on multi-agent particle swarm optimization algorithm. *Sustainability*, 11:1973, 04 2019. 10.3390/su11071973.

[14] Reza Fachrizal, Mahmoud Shepero, Magnus Åberg, and Joakim Munkhammar. Optimal pv-ev sizing at solar powered workplace charging stations with smart charging schemes considering self-consumption and self-sufficiency balance. *Applied Energy*, 307:118139, 2022. 10.1016/j.apenergy.2021.118139.

[15] Mohammad Jafari, Zahra Malekjamshidi, Jianguo Zhu, and Mohammad-Hassan Khooban. A novel predictive fuzzy logic-based energy management system for grid-connected and off-grid operation of residential smart microgrids. *IEEE Journal of Emerging*

and Selected Topics in Power Electronics, 8(2):1391–1404, 2020. 10.1109/JESTPE.2018.2882509.

[16] Sheikh Jakir Hossain, Biswajit Dipan Biswas, Rojan Bhattarai, Muhammad Ahmed, Sherif Abdelrazek, and Sukumar Kamalasadan. Operational value-based energy storage management for photovoltaic (pv) integrated active power distribution systems. *IEEE Transactions on Industry Applications*, 55(5):5320–5330, 2019. 10.1109/TIA.2019.2920229.

[17] Ashfaq Ahmad and Jamil Yusuf Khan. Roof-top stand-alone pv microgrid: A joint real-time bes management, load scheduling and energy procurement from a peaker generator. *IEEE Transactions on Smart Grid*, 10(4):3895–3909, 2019. 10.1109/TSG.2018.2842757.

[18] Anjeet Verma, Bhim Singh, Ambrish Chandra, and Kamal Al-Haddad. An implementation of solar pv array based multifunctional ev charger. *IEEE Transactions on Industry Applications*, 56(4):4166–4178, 2020. 10.1109/TIA.2020.2984742.

[19] S. Jithin and T. Rajeev. Investigation on stability of dc microgrid for large-scale electric vehicle charging station deployment. In Gayadhar Panda, R. T. Naayagi, and Sukumar Mishra, editors, *Sustainable Energy and Technological Advancements*, pages 637–646, Singapore, 2022. Springer Singapore.

[20] Jithin S and Rajeev T. A hybrid virtual synchronous machine topology for improved microgrid stability. In *2021 4th Biennial International Conference on Nascent Technologies in Engineering (ICNTE)*, pages 1–6, 2021. 10.1109/ICNTE51185.2021.9487777.

[21] Jun Hou, Ziyou Song, Heath F. Hofmann, and Jing Sun. Control strategy for battery/flywheel hybrid energy storage in electric shipboard microgrids. *IEEE Transactions on Industrial Informatics*, 17(2):1089–1099, 2021. 10.1109/TII.2020.2973409.

Biographies

S. Jithin received the B.Tech. and M.Tech. degrees in Electrical and Electronics Engineering from the University of Calicut, Kozhikode, India, and the APJ Abdul Kalam Technological University, Kerala, India, in 2015 and 2018, respectively. He is currently working toward the Ph.D. degree from the College of Engineering, Trivandrum, India, under APJ Abdul Kalam Technological University. His research interests include hybrid AC/DC microgrids, electric vehicles and their integration into smart grids.

T. Rajeev received the M.Tech. degree in Electrical and Electronics Engineering from the University of Kerala, Thiruvananthapuram, India, in 2009 and the Ph.D. degree in Electrical Engineering from the National Institute of Technology Calicut, Kozhikode, India, in 2015. He is currently working as a Professor in Electrical Engineering Department, College of Engineering, Trivandrum, India. His research interests include the design and operation of microgrid and smart grids, electric vehicle, and hybrid energy systems.